Published in final edited form as:
Nanotechnology. 2011 March 18; 22(11): 115101.

Effect of Particle Size, Density and Shape on Margination of Nanoparticles in Microcirculation

Randall Toy[1,2], **Elliott Hayden**[1], **Christopher Shoup**[1], **Harihara Baskaran**[1,3], and **Efstathios Karathanasis**[1,2,*]

[1]Department of Biomedical Engineering, Case Western Reserve University, Cleveland, OH 44106

[2]Department of Radiology and Case Center for Imaging Research, Case Western Reserve University, Cleveland, OH 44106

[3]Department of Chemical Engineering, Case Western Reserve University, Cleveland, OH 44106

Abstract

In the recent past, remarkable advances in nanotechnology have generated nanoparticles of different shapes and sizes, which have been shown to exhibit unique properties suitable for biomedical applications such as cancer therapy and imaging. Obviously, all nanoparticles are not made equal. This becomes evident when we consider their transport behavior under blood flow in microcirculation. In this work, we evaluated the effect of critical physical characteristics such as the particle shape, size and density on a nanoparticle's tendency to marginate towards the vessel walls in microcirculation using an *in vitro* model. The wall-deposition of nanoparticles was tested in a fibronectin-coated microfluidic channel at a physiologically relevant flow rate. Different classes of nanoparticles (liposome, metal particles) of different sizes (60–130 nm), densities (1–19 g/mL) and shapes (sphere, rod) displayed significantly different deposition as a result of different margination rates. The smaller-sized and the oblate-shaped particles displayed a favorable behavior as indicated by their higher margination rates. Notably, the particle density showed an even more essential role, as it was observed that the lighter particles marginated significantly more. Since nanoparticles must escape the flow in order to approach the vascular bed and subsequently extravascular components for meaningful interactions, the design of nanoparticles strongly affects their margination, a key factor for their ultimate *in vivo* effectiveness.

Keywords

Margination; drifting; nanoparticles; microfluidic channel; tumor microcirculation; nanoparticle shape; nanoparticle size; nanoparticle density

1. Introduction

Being at the crossroads of chemistry, material science, engineering, and medicine, nanomedicine exploits the unique features of nanoparticles to design improved anticancer interventions (Yezhelyev *et al.*, 2006; Lasic and Papahadjopoulos, 1995). An advantage of being at the nanoscale is the ability to combine more than one function by enabling the design of multifunctional nanoparticles that seek (*i.e.* passive and active targeting), image (*i.e.* loaded with contrast agents), and damage (*i.e.* loaded with anticancer agents) (Service, 2005). Not surprisingly, this has led to the development of numerous types of nanoparticles

*Author to whom correspondence should be addressed: Efstathios Karathanasis, Ph.D. Assistant Professor, Departments of Biomedical Engineering and Radiology, Case Western Reserve University, Wickenden Bldg. MS 7207, 10900 Euclid Ave, Cleveland, OH 44106, Phone: 216.844.5281; Fax: 216.844.4987; stathis@case.edu.

for imaging and therapy such as liposomes, dendrimers, other lipid-based and polymeric nanoparticles, and metal nanoparticles (*e.g.* iron oxide and gold) (Ferrari, 2005). While most of the early generation particles were spherical, recent advances have exploited the engineerability of nanoparticles to shape them with defined geometrical, physical and chemical properties. For example, oblate- and rod-shaped nanostructures have been fabricated suitable for biomedical applications such as nanorods (Huang *et al.*, 2006), nanochains (Sardar and Shumaker-Parry, 2008), nanoworms (Park *et al.*, 2009; Park *et al.*, 2008), and nanonecklaces (Dai *et al.*, 2005). Evidently, nanotechnology has the ability to shape matter into various classes of particles with very different characteristics including size, shape, density, and surface chemistry.

Notably, those characteristics of nanoparticles have been shown to play a central role in their transport in the abnormal tumor microcirculation (Lee *et al.*, 2009). Successful delivery of nanoscale agents requires that the particle enters the tumor microcirculation, navigates through the tumor leaky vasculature into the tumor interstitium and is delivered to cytoplasmic targets in cancer cells. However, nanoparticles en route to their target face numerous biobarriers created by the tumor abnormal physiology. Abnormal tumor features, including physically compromised vasculature, erratic blood flow, abnormal extracellular matrix, and high interstitial fluid pressure, can limit the effective delivery of nanoparticles.

One of the pivotal steps dictating the intratumoral fate of nanoparticles is their margination (*i.e.* lateral drift) towards the blood vessel walls. Near-the-wall margination is not just desirable; it is required for the particle to be able to interact with the tumor vascular bed. Subsequently, the particle will have the chance to either target tumor-specific vascular biomarkers or extravasate through the tumor leaky endothelium into the tumor interstitium. Even though tumors display blood flows significantly slower than that of normal circulation, nanoparticles, due to their size, are primarily transported in the tumor microcirculation via convective means and therefore margination is not favored, which is not the case for small molecules. In order for a particle to escape the blood flow streamlines resulting in margination, forces that depend on the particle characteristics such as gravity, buoyancy, diffusion or torque are required (Gavze and Shapiro, 1998; Hogg, 1994). Apparently, only the latter two factors are important for nanoparticle margination (Gentile *et al.*, 2008a; Gentile *et al.*, 2008b). Therefore, key characteristics of nanoparticles, such as density, size and shape, have important consequences on the delivery of nanoparticles to tumors.

In a recent experimental study (Gentile *et al.*, 2008b), 50 nm polystyrene nanospheres exhibited significantly higher margination on a parallel plate flow chamber compared to 100 or 200 nm spheres. Other computational and experimental studies have shown that oblate-shaped particles encourage margination due to torque forces (Decuzzi *et al.*, 2009; Gentile *et al.*, 2008a). In addition, the tumor hemodynamics and vascular permeability has also been shown to significantly influence the transport of nanoparticles (Decuzzi *et al.*, 2006; Decuzzi and Ferrari, 2008; Gentile *et al.*, 2008c). However, it is well-known that tumors represent a very heterogeneous population with several parameters varying not only among same type of tumors but even spatially within the same tumor (Fukumura and Jain, 2007; Hobbs *et al.*, 1998; Yuan *et al.*, 1996; Karathanasis *et al.*, 2009a; Karathanasis *et al.*, 2009b). Taking under consideration this variability, one intriguing argument is to consider that each tumor displays unique biobarriers to nanoparticles.

To understand the fundamental relationship of flow with particle characteristics, in this work we studied the margination of nanoparticles in microchannels (175 μm wide) under physiologic flow rates expected in tumor microcirculation. The effect of particle density (ρ_p), size and shape were evaluated using different classes of nanoparticles (shown in Table 1): 1) spherical liposomes (ρ_p~1) with diameters of 65, 100, and 130 nm, 2) a spherical

iodine-loaded liposome (ρ_p~2.4) with a diameter of 65 nm, 3) an iron oxide nanoparticle (ρ_p~5) with a diameter of 60 nm, 4) a gold nanoparticle (ρ_p~19) with a diameter of 60 nm, and (5) a gold nanorod (ρ_p~19) with a length of 56 nm and an aspect ratio of ~0.45. Another important aspect of this study was that each nanoparticle population exhibited a very narrow size distribution, the same surface coating (*i.e.* polyethylene glycol), and nearly zero surface charge.

2. Materials and Methods

2.1. Materials

The phospholipid 1,2-dipalmitoyl-sn-glycero-3-phosphocholine (DPPC) was purchased from Genzyme Pharmaceuticals (Cambridge, MA). DSPE-PEG_{2000}-NH_2 was obtained from Laysan Bio (Arab, AL). Cholesterol was purchased from Sigma (St. Louis, MO). Gold nanospheres and gold nanorods were purchased from Nanopartz Inc. (Loveland, CO). Iron oxide nanoparticles were obtained from Ocean Nanotech (Springdale, AR). Alexa Fluor 488 N-succinimidyl ester was obtained from Invitrogen (Carlsbad, CA). The rest of the reagents were of analytical grade (Fisher Scientific, Cleveland, OH).

2.2. Liposomes

A lipid composition of DPPC, cholesterol and DSPE-PEG_{2000}-NH_2 in the molar ratio of 55: 40: 5 respectively was used. The lipids were dissolved in ethanol and hydrated with phosphate buffered saline (PBS) at 60°C followed by sequential extrusion in a Lipex Biomembranes Extruder (Northern Lipids, Vancouver, Canada), to size the liposomes to 130 or 100 or 65 nm. Samples were then dialyzed for two days against PBS using a 100 kDa molecular weight cutoff dialysis membrane.

A particle density of 2.4 g/mL was achieved by encapsulating a concentrated iodinated solution into the liposome using established methods (Karathanasis *et al.*, 2009a; Karathanasis *et al.*, 2009b). Briefly, a highly concentrated iodine solution (650 mg I/mL) was prepared by dissolving iodixanol powder (lyophilized from Visipaque 320; GE Healthcare, Milwaukee, WI) in ultrapure water under stirring and heating at 70°C. The lipid composition was similar to that described previously. The liposomes were extruded to size them to 65 nm. Free, un-encapsulated iodine was replaced by PBS using a 2-day dialysis. The final iodine levels were quantified through spectrophotometry at 245 nm.

Finally, the liposome formulations were fluorescently tagged by conjugating Alexa 488 NHS on the amines at the distal end of the surface PEG polymer. An excess (2×) of the fluorophore was used to assure coverage of all the amines on the surface of the particle (~900, 2000, 3500 amines per 65, 100, 130 nm liposome respectively). Free fluorophore was removed by dialysis against PBS for two days. We employed a typical 5 mol% PEG coverage which has been shown to provide *in vitro* and *in vivo* stability (Johnsson and Edwards, 2003; Klibanov *et al.*, 1990; Israelachvili, 1992; Lasic and Martin, 1995). The sizes of the liposome formulations were confirmed by dynamic light scattering (DLS) with a Brookhaven Particle Size and Zeta Potential Analyzer (Brookhaven Instruments, Holtsville, NY). Their zeta potentials were measured using the Brookhaven Particle Size and Zeta Potential Analyzer.

2.3. Metal nanoparticles

The metal particles were obtained from commercial vendors as mentioned in the materials section. Gold nanospheres displayed a diameter of 60 nm with very low size dispersity which was confirmed by TEM images and DLS measurement. The gold nanorod's length and transverse diameter were 56 and 25 nm, respectively. The surface of the gold sphere and

rod were decorated with about 70 and 200 amines per particle. The iron oxide nanospheres exhibited a core diameter of 50 nm (based on TEM) and a hydrodynamic diameter of 60 nm (based on DLS measurements). The modification of the surface with a PEG coating has been well-documented for the gold sphere and rod (Dreaden *et al.*, 2009; Akiyama *et al.*, 2009) and the metal nanoparticles (Yang *et al.*, 2008; Yang *et al.*, 2009). Conjugation of Alexa 488 onto the surface of the particles was achieved using a method similar to that of liposomes followed by measurement of the zeta potential.

2.4. Fabrication of PDMS Microchannel Devices

Standard photolithography techniques were used to transfer the design of the flow microchannel to negative templates of photoresist (SU-8 2075) on a 4" silicon wafer (Janakiraman *et al.*, 2007). These templates were then used to embed the designs in PDMS (Whitesides *et al.*, 2001). PDMS has advantages such as ease of availability, fabrication and manipulation. The channel had a length of 5 cm and a cross section with dimensions of 175×100 μm (WxH). Fluid access to the networks was provided via 1 mm OD Silastic tubing connected to the PDMS membrane. Phase contrast and relief contrast techniques were used to measure and verify channel dimensions of the PDMS networks.

2.5. Experimental setup

Image acquisition was performed using an Olympus IX-71 inverted fluorescent microscope (Olympus Corporation, USA). All acquired images were 12-bit grayscale and taken at 20X magnification. At every imaging time point, three regions of interest were imaged at different portions of the microchannel (entrance, center, and exit). PDMS microchannel devices were incubated with fibronectin at 100 μg/mL overnight. Channels with fibronectin were flushed thoroughly with PBS before the start of the experiment. Fluorescent images of the channel were acquired before the introduction of nanoparticles. Then, nanoparticles at a concentration of 3×10^{11} particles/mL were infused into the microchannels with a Harvard syringe pump (Harvard Apparatus, Holliston, MA) at a flow rate of 50 μL/min for 8 minutes. Following nanoparticle flow, channels were washed with PBS at a flow rate of 50 μL/min for 30 minutes. Images were acquired in each phase to qualitatively assess particle deposition during the experiment. The non-adherent nanoparticles were collected from the outlet of the microchannel during both the nanoparticle flow and PBS wash phase of the experiment. Adherent nanoparticles were collected separately by flushing the system with ethanol. Particle concentration was measured using a fluorescent plate reader (BIOTEK, Winooski, VT: excitation wavelength = 485 nm, emission wavelength= 528 nm). The volumes of the collected nanoparticles were measured so that the number of adherent and non-adherent nanoparticles could be calculated from mass balance. Percent deposition was then calculated by dividing the total number of adherent nanoparticles by the sum of the number of adherent and non-adherent nanoparticles, multiplied by 100. It should be noted that we performed pilot studies to evaluate potential photobleaching of the fluorophore and whether this should be taken into account. Alexa-488 photobleaching was assessed by analyzing images of a channel filled with fluorescently-tagged liposomes under static conditions (no flow), exposed continuously to light from the microscope, acquired over a 20 minute time period. It was found that the fluorescence decreased approximately 1% per minute of direct light exposure. In each microchannel experiment, overall image acquisition time was less than 2 minutes. Since quantification of the nanoparticle deposition rates were based on the collection of a large number of particles from the entire channel, the effect of photobleaching on the fluorescence measurements was considered negligible.

2.6. Statistical Analysis

To determine the significance in the differences between groups, an unpaired one-tailed Student *t* test analysis was performed (SPSS 15, Chicago, IL). A p-value less than 0.05 was used to confirm significant differences.

3. Results and Discussion

3.1. Preliminary evaluation of the microchannel setup

In order to study the tendency of nanoparticle margination in microcirculation, we fabricated a microfluidic device consisting of a straight 5 cm-long microchannel with dimensions of 100 × 175 μm (height × width), which replicates the dimensions of an arteriole or venule (Ganong, 2003; Less *et al.*, 1991). To truly evaluate the relation of the physical characteristics of a nanoparticle to its margination under flow, we need a surface which captures marginating particles in a broad non-specific manner. Therefore, active targeting of a ligand-presenting particle to a "receptor-coated" microchannel would be undesirable as the shape and size of particles results in a variable degree of binding strength for each particle (Decuzzi and Ferrari, 2006), and therefore delineation of the chemical effects from the physical effects will be difficult. To avoid undesirable specific binding events, the channel was coated with fibronectin, an extracellular matrix protein that has been shown to significantly increase cell attachment on PDMS (Lee *et al.*, 2004; Pankov and Yamada, 2002; Wang *et al.*). It has been shown that cells can adhere to a fibronectin treated PDMS surface when the surface is incubated with a solution of 10 μg/mL fibronectin (Lee *et al.*, 2004). To further ensure adhesion of the nanoparticles to the wall upon contact, we incubated the microchannel with an excess of fibronectin (*i.e.* 100 μg/mL). Previous studies have shown that fibronectin at these concentrations forms a layer of 4-5 nm thick, which is insufficient to influence the flow pattern within the device (Al-Jawad *et al.*, 2009).

Figure 1 shows a schematic of the experimental setup. To study the adhesive strength of the fibronectin-coated microchannel, the nanoparticle suspension was infused via a syringe pump into a PBS-filled microchannel at a flow rate of 50 μL/min, which is the expected blood flow in a vessel with the microchannel's dimensions (Ganong, 2003). The nanoparticle suspension was switched to PBS to flush out the nanoparticles that were deposited on the walls. In order to optimize the experimental conditions, we initially asked three important questions: (1) How long did it take for the nanoparticles to reach a constant concentration in the lumen during the initial transition time? (2) What was the required time for deposition of nanoparticles to completely cover the channel's surface (*i.e.* saturation of the channel's surface)? (3) Once the nanoparticles deposited on the walls, did they detach and return back to the flow? Fluorescence microscopy was used to semi-quantitatively interrogate the fate of the fluorescently tagged nanoparticles in the channel in a real-time fashion. Figure 2 shows results from a 'saturation experiment' performed with the 65 nm liposomes. Images were acquired from the center of the microchannel. Fluorescence signal was found by determining the average pixel value of an ROI drawn around one segment of a microchannel (175 × 400 μm). In the beginning of the experiment, the nanoparticles required about 5 minutes to reach a constant concentration in the lumen of the channel. The initial sharp signal increase due to the transition from PBS to nanoparticles in the lumen was followed by a substantially slower increase in the fluorescence signal. The latter slower increase suggests continuous deposition of nanoparticles on the channel walls. In the third phase, the removal of the nanoparticles from the lumen of the channel with PBS caused a rapid decrease in the signal. Once the channel was completely filled with PBS, it was observed that the signal from the channel remained constant (t=40–60 min). Importantly, the levels of the signal were significantly higher compared to the background (*i.e.* t<0) indicating adhesion of particles to the lumen wall. Not surprisingly, ethanol, which

solubilizes liposomes, was able to completely clean the channel as indicated by the return of the signal to the background levels. Therefore, we concluded the nanoparticles adhered on the fibronectin coating without detaching and returning back to the flow. In the bottom of Figure 2, representative microscopy images are shown. It should be noted that the saturation experiments for the other nanoparticles yielded similar trends.

It should also be noted that we employed microchannels with a rectangular cross-section in contrast to the circular one of the microvasculature. The flow profile in channels of rectangular or circular cross-section is expected to exhibit dissimilar patterns. The primary difference is anticipated to be in the 'dead space' of the corners of the rectangular channel. Using fluorescence microscopy, we interrogated the topology of the nanoparticle deposition in the microchannels with rectangular cross-section and we detected negligible signal from the corners indicating that few particles deposited in these regions. Therefore, we can conclude that our findings can be fairly extrapolated to cylindrical microchannels as well. Notably, in an ongoing project we are working on the fabrication of cylindrical microchannels with more complex structure (i.e. more bifurcations).

Furthermore, it should be noted that all the nanoparticles used in this study displayed a very mild charge. The fluorescently tagged liposomes and gold particles displayed a slightly positive zeta potential (about 5 mV), whereas the iron particles exhibited a slightly negative zeta potential (about −10 mV). Therefore, the nanoparticle margination and deposition on the fibronectin-coated channel could not be attributed to ionic interactions.

3.2. Effect of nanoparticle size

The concentration of nanoparticles used in this study was chosen based on a representative dose of a clinically used nanoparticle chemotherapeutic (*i.e.* liposomal doxorubicin (Lasic and Papahadjopoulos, 1995)). An intravenous dose of 10 mg doxorubicin per kilogram of body weight (Campos, 2003) results in an initial concentration of about 5×10^{12} liposomes per mL of blood. In our experiments, the number of particles per mL for all the nanoparticles was fixed at about 10% of the initial "clinical" concentration (*i.e.* 3×10^{11} nanoparticles/mL).

Based on the results from saturation experiments, we chose 8 minutes as the adhesion time for subsequent margination and adhesion experiments. The nanoparticles were allowed to run through the system for 8 min followed by PBS flushing and finally ethanol wash. The channel was semi-quantitatively monitored in real-time using fluorescence microscopy as before. The timeline of a typical margination and adhesion experiment with the 65 nm liposomes is shown in Figure 3 based on the semi-quantitative microscopy. Upon collection of only the wall-deposited nanoparticles using a final ethanol wash, the deposition of the nanoparticles was quantified using a fluorescence reader.

In order to evaluate the dependence of margination on the size of the particles at the nanoscale, three different liposome formulation encapsulating PBS were tested. The size distributions shown in Figure 4a indicate that each liposome formulation represented a distinct population with a narrow size distribution. Not surprisingly, the smaller liposomes exhibited the highest deposition (Figure 4b). For margination to occur, the particle has to escape the flow streamline. Since the contribution of buoyancy or gravity can be assumed negligible for these nanoparticles (Lee *et al.*, 2009), diffusion of the particle should outweigh its momentum for margination and deposition to occur. Since the diffusion coefficient is inversely proportional to the size of the particle (Table 2), the higher diffusion component of the smaller spheres is implied to enhance their margination.

3.3. Effect of nanoparticle density and shape

The effect of particle momentum was further examined by comparing same-sized particles with different masses. Based on the Stokes-Einstein equation, particles with the same diameter should have the same diffusion coefficient (as shown in Table 2). Therefore, nanospheres with a diameter of 65 nm of different constituting materials will diffuse equally. However, the momentum (and inertia) of particles of the same size strongly depends on the particle's density. While the degree of diffusion of every 65 nm sphere was the same, at similar flow rates, the gold sphere is expected to "carry" more momentum due to its large density. Therefore, a gold sphere should face more difficulty to marginate compared to a particle of the same size but lower density (*e.g.* liposome). The relative contribution of diffusion to momentum can be expressed by the inverse of a modified Peclet number, as shown in the right column of Table 2 where ρ_p is the particle density, ρ is the density of water, L is the length of the channel, u is the maximum mean fluid velocity, and D is the diffusion coefficient of the particle. As expected, increases in this dimensionless number as a result of density changes led to an increase in deposition.. Figure 5a shows a clear dependence of the deposition on the particle density. Notably, a very "light" particle (*e.g.* liposome with ρ_p~1 g/mL) can result in 57 times greater deposition than a very "heavy" one (*e.g.* gold particle with ρ_p~19 g/mL). In addition, particles that consist of the same shell (*i.e.* liposome) but encapsulate material of different density (*e.g.* water versus concentrated iodine) resulted in significant differences in deposition.

We should mention that we compared soft and hard nanoparticles. The axial migration of liposomes (soft particles) depends on their elasticity, since deformability of the liposome membrane can lead to a lift force under flow. However, the liposomes used in our studies, DPPC-membrane liposomes are known to be very rigid particles (and thus have long circulation times). The Young's modulus of DPPC liposomes is about 110 MPa and the bending rigidity is about 330 k_BT. We, therefore, did not consider this phenomenon to contribute to our results.

To further investigate the effect of momentum on margination, we hypothesized that a faster flow rate should result in a decrease of nanoparticle margination. Theoretically, a quadrupling in the flow rate (*i.e.* 200 μL/min) should decrease the contribution of diffusion and subsequently margination by a factor of 4 as indicated by the dimensionless number (*i.e.* diffusion/momentum) in Table 2. Not surprisingly, Figure 5b shows that the deposition of a 65 nm liposome was about 3 times lower at the faster flow rate. One could hypothesize that the deposition under the slower and the faster flow rates are similar. The lower deposition at the faster flow rate could actually be attributed to the fact that the adhesive strength of fibronectin is not sufficient to retain deposited nanoparticles onto the channel's walls under the faster flow. It should be noted that we performed a saturation experiment under the faster flow rate, which showed no detachment, and therefore we can conclude that there is lower margination at 200 μL/min.

The effect of shape has also been shown to play a critical role in the margination of nanoparticles (Gentile *et al.*, 2008a; Lee *et al.*, 2009). In contrast to spherical particles, oblate-shaped particles are subjected to torques resulting in tumbling and rotation (Gavze and Shapiro, 1998; Lee *et al.*, 2009). These complex dynamics of non-spherical particles cause translational as well as rotational motions. In order to obtain a comparative indication of the effect of shape, the deposition of a gold nanorod was tested and compared against a gold sphere with comparable diameter (Figure 5c). Similarly to previous theoretical and experimental studies (Gentile *et al.*, 2008a; Lee *et al.*, 2009), the rod displayed about 8 times higher deposition than the sphere.

In Figure 6, the overall performance of all the nanoparticles is shown. Taking under consideration that the experimental conditions were identical for all the particles, the influence of the physical characteristics of the particles can be appreciated. While the size and shape has been shown to strongly affect margination, the particle density seems to play an even more essential role. Within the short timeframe of the experiment (*i.e.* 8 min), the "lighter" sphere (liposome encapsulating PBS) displayed about 57 and 7 times higher deposition than the "heavier" gold sphere and rod of similar dimensions, respectively. It should be noted that the *in vivo* performance of a nanoscale agent depends on many complex factors, such as its blood residence time, and the loading of active compound (*e.g.* therapeutic or imaging agent). However, the relation of margination with the particle physical characteristics should not be neglected in the design of nanoparticles as they might be key contributors to the *in vivo* outcome.

4. Conclusions

In conclusion, a systematic *in vitro* analysis provided valuable findings regarding the margination tendency of flowing nanoparticles. In good agreement with previous studies (Gentile *et al.*, 2008a; Lee *et al.*, 2009), the smaller particles and rods favored margination. Notably, the experimental protocol allowed us to resolve differences in margination tendency of particles at the nanoscale (*i.e.* about 30 nm difference in the diameter of nanoparticles). More importantly, the particle density had an even stronger influence, as the lighter particles marginated further than the denser particles. Finally, the effect of particle size and density on margination and deposition can be described by a single dimensionless number (inverse of modified Peclet number). While the current experimental setup generated valuable conclusions, the transport of nanoparticle in a medium resembling the complexity of blood using a microchannel network of more than one channel is a subject of ongoing studies.

Acknowledgments

The authors would like to thank Pubudu Peiris for useful discussions. The study is supported in part by a grant from the National Institutes of Health, R01-EB006203 (HB).

References

Akiyama Y, Mori T, Katayama Y, Niidome T. The effects of PEG grafting level and injection dose on gold nanorod biodistribution in the tumor-bearing mice. J Control Release. 2009; 139:81–4. [PubMed: 19538994]

Al-Jawad M, Fragneto G, Liu J, Chang SR, Clarkson B. Fibronectin adsorption studied using neutron reflectometry and complementary techniques. Eur Phys J E Soft Matter. 2009; 30:175–9. [PubMed: 19551415]

Campos S. Liposomal anthracyclines: adjuvant and neoadjuvant therapy for breast cancer. Oncologist. 2003; 8(Suppl 2):10–6. [PubMed: 13679591]

Dai Q, Worden JG, Trullinger J, Huo Q. A "nanonecklace" synthesized from monofunctionalized gold nanoparticles. J Am Chem Soc. 2005; 127:8008–9. [PubMed: 15926813]

Decuzzi P, Causa F, Ferrari M, Netti PA. The effective dispersion of nanovectors within the tumor microvasculature. Ann Biomed Eng. 2006; 34:633–41. [PubMed: 16568349]

Decuzzi P, Ferrari M. The adhesive strength of non-spherical particles mediated by specific interactions. Biomaterials. 2006; 27:5307–14. [PubMed: 16797691]

Decuzzi P, Ferrari M. Design maps for nanoparticles targeting the diseased microvasculature. Biomaterials. 2008; 29:377–84. [PubMed: 17936897]

Decuzzi P, Pasqualini R, Arap W, Ferrari M. Intravascular delivery of particulate systems: does geometry really matter? Pharm Res. 2009; 26:235–43. [PubMed: 18712584]

Dreaden EC, Mwakwari SC, Sodji QH, Oyelere AK, El-Sayed MA. Tamoxifen-poly(ethylene glycol)-thiol gold nanoparticle conjugates: enhanced potency and selective delivery for breast cancer treatment. Bioconjug Chem. 2009; 20:2247–53. [PubMed: 19919059]

Ferrari M. Cancer nanotechnology: opportunities and challenges. Nat Rev Cancer. 2005; 5:161–71. [PubMed: 15738981]

Fukumura D, Jain RK. Tumor microenvironment abnormalities: causes, consequences, and strategies to normalize. Journal of cellular biochemistryi. 2007; 101:937–49.

Ganong, WF. Review of Medical Physiology. New York: Lange Medical Books/McGraw-Hill, Medical Publishing Division; 2003.

Gavze E, Shapiro M. Motion of inertial spheroidal particles in a shear flow near a solid wall with special application to aerosol transport in microgravity. Journal of Fluid Mechanics. 1998; 371:59–79.

Gentile F, Chiappini C, Fine D, Bhavane RC, Peluccio MS, Cheng MM, Liu X, Ferrari M, Decuzzi P. The effect of shape on the margination dynamics of non-neutrally buoyant particles in two-dimensional shear flows. J Biomech. 2008a; 41:2312–8. [PubMed: 18571181]

Gentile F, Curcio A, Indolfi C, Ferrari M, Decuzzi P. The margination propensity of spherical particles for vascular targeting in the microcirculation. J Nanobiotechnology. 2008b; 6:9. [PubMed: 18702833]

Gentile F, Ferrari M, Decuzzi P. The transport of nanoparticles in blood vessels: the effect of vessel permeability and blood rheology. Ann Biomed Eng. 2008c; 36:254–61. [PubMed: 18172768]

Hobbs SK, Monsky WL, Yuan F, Roberts WG, Griffith L, Torchilin VP, Jain RK. Regulation of transport pathways in tumor vessels: role of tumor type and microenvironment. Proc Natl Acad Sci U S A. 1998; 95:4607–12. [PubMed: 9539785]

Hogg AJ. The inertial migration of non-neutrally buoyant spherical particles in two-dimensional shear flows. Journal of Fluid Mechanics. 1994; 272:285–318.

Huang X, El-Sayed IH, Qian W, El-Sayed MA. Cancer cell imaging and photothermal therapy in the near-infrared region by using gold nanorods. JACS. 2006; 128:2215–120.

Israelachvili, J. Intermolecular and surface forces. London: Academic Press; 1992. p. 395-421.

Janakiraman V, Kienitz BL, Baskaran H. Lithography techniques for topographical micropatterning of collagen-glycosaminoglycan membranes for tissue engineering applications. Journal of Medical Devices. 2007; 1:233–7. [PubMed: 19823602]

Johnsson M, Edwards K. Liposomes, disks, and spherical micelles: aggregate structure in mixtures of gel phase phosphatidylcholines and poly(ethylene glycol)-phospholipids. Biophys J. 2003; 85:3839–47. [PubMed: 14645073]

Karathanasis E, Chan L, Karumbaiah L, McNeeley K, D'Orsi CJ, Annapragada AV, Sechopoulos I, Bellamkonda RV. Tumor vascular permeability to a nanoprobe correlates to tumor-specific expression levels of angiogenic markers. PLoS ONE. 2009a; 4:e5843. [PubMed: 19513111]

Karathanasis E, Suryanarayanan S, Balusu SR, McNeeley K, Sechopoulos I, Karellas A, Annapragada AV, Bellamkonda RV. Imaging nanoprobe for prediction of outcome of nanoparticle chemotherapy by using mammography. Radiology. 2009b; 250:398–406. [PubMed: 19188313]

Klibanov AL, Maruyama K, Torchilin VP, Huang L. Amphipathic polyethyleneglycols effectively prolong the circulation time of liposomes. FEBS Lett. 1990; 268:235–7. [PubMed: 2384160]

Lasic, D.; Martin, F. Stealth Liposomes. CRC Press Inc; 1995.

Lasic DD, Papahadjopoulos D. Liposomes revisited. Science. 1995; 267:1275–6. [PubMed: 7871422]

Lee JN, Jiang X, Ryan D, Whitesides GM. Compatibility of mammalian cells on surfaces of poly(dimethylsiloxane). Langmuir. 2004; 20:11684–91. [PubMed: 15595798]

Lee SY, Ferrari M, Decuzzi P. Shaping nano-/micro-particles for enhanced vascular interaction in laminar flows. Nanotechnology. 2009; 20:495101. (11pp). [PubMed: 19904027]

Less JR, Skalak TC, Sevick EM, Jain RK. Microvascular architecture in a mammary carcinoma: branching patterns and vessel dimensions. Cancer Res. 1991; 51:265–73. [PubMed: 1988088]

Pankov R, Yamada KM. Fibronectin at a glance. J Cell Sci. 2002; 115:3861–3. [PubMed: 12244123]

Park JH, von Maltzahn G, Zhang L, Derfus AM, Simberg D, Harris TJ, Ruoslahti E, Bhatia SN, Sailor MJ. Systematic surface engineering of magnetic nanoworms for in vivo tumor targeting. Small. 2009; 5:694–700. [PubMed: 19263431]

Park JH, von Maltzahn G, Zhang LL, Schwartz MP, Ruoslahti E, Bhatia SN, Sailor MJ. Magnetic iron oxide nanoworms for tumor targeting and imaging. Advanced Materials. 2008; 20:1630–5. [PubMed: 21687830]

Sardar R, Shumaker-Parry JS. Asymmetrically functionalized gold nanoparticles organized in one-dimensional chains. Nano Letters. 2008; 8:731–6. [PubMed: 18269261]

Service RF. Materials and biology. Nanotechnology takes aim at cancer. Science. 2005; 310:1132–4. [PubMed: 16293748]

Wang L, Sun B, Ziemer KS, Barabino GA, Carrier RL. Chemical and physical modifications to poly(dimethylsiloxane) surfaces affect adhesion of Caco-2 cells. J Biomed Mater Res A. 93:1260–71. [PubMed: 19827104]

Whitesides GM, Ostuni E, Takayama S, Jiang X, Ingber DE. Soft lithography in biology and biochemistry. Annu Rev Biomed Eng. 2001; 3:335–73. [PubMed: 11447067]

Yang L, Mao H, Wang YA, Cao Z, Peng X, Wang X, Duan H, Ni C, Yuan Q, Adams G, Smith MQ, Wood WC, Gao X, Nie S. Single chain epidermal growth factor receptor antibody conjugated nanoparticles for in vivo tumor targeting and imaging. Small. 2008; 133:154–60.

Yang L, Peng X, Wang A, Wang X, Cao Z, Ni C, Karna P, Zhang X, Wood WC, Gao X, Nie Sand Mao H. Receptor-targeted nanoparticles for in vivo imaging of breast cancer. Clinical Cancer Research. 2009; 15:4722–32. [PubMed: 19584158]

Yezhelyev MV, Gao X, Xing Y, Al-Hajj A, Nie S, O'Regan RM. Emerging use of nanoparticles in diagnosis and treatment of breast cancer. The lancet oncology. 2006; 7:657–67. [PubMed: 16887483]

Yuan F, Chen Y, Dellian M, Safabakhsh N, Ferrara N, Jain RK. Time-dependent vascular regression and permeability changes in established human tumor xenografts induced by an anti-vascular endothelial growth factor/vascular permeability factor antibody. Proc Natl Acad Sci U S A. 1996; 93:14765–70. [PubMed: 8962129]

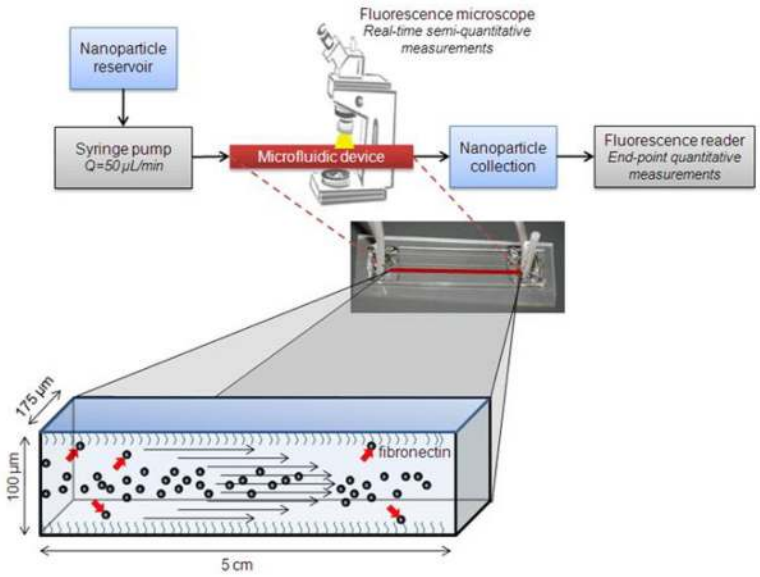

Figure 1.
Schematic of the experimental setup.

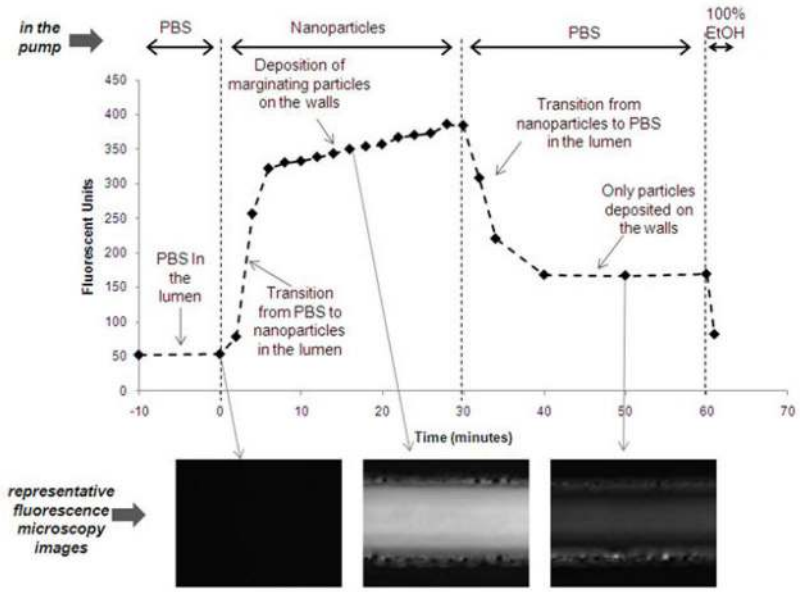

Figure 2. A typical saturation experiment is shown for the 65 nm liposomes

At t<0, the microchannel was filled with PBS. At t=0, 3×10^{11} nanoparticles/mL were flowed through the microchannel at 50 μL/min. At t=30 min, the lumen was continuously flushed with PBS for 30 minutes. At t=60 min, the microchannel was flushed with ethanol. A series of 12-bit images were captured using a fluorescence microscope which enabled the dynamic semi-quantitative analysis showed in the plot. Representative images of each phase are shown in the bottom.

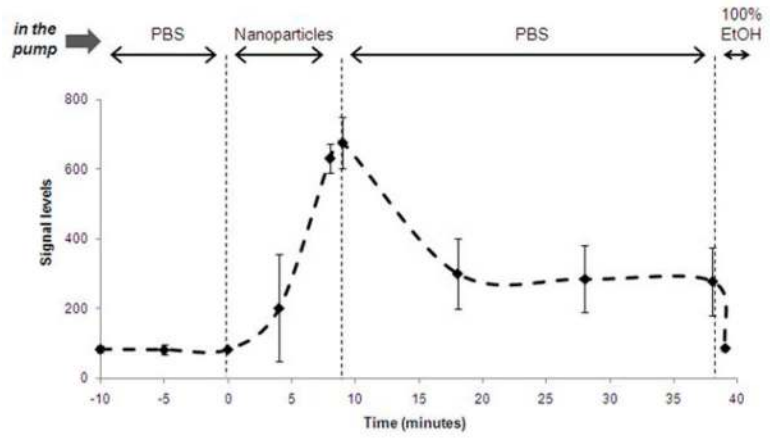

Figure 3. A typical margination experiment is shown for the 65 nm liposomes

At t<0, the microchannel was filled with PBS. At t=0, 3×10^{11} nanoparticles/mL were flowed through the microchannel at 50 μL/min. At t=8 min, the lumen was continually flushed with PBS for 30 minutes. A series of 12-bit images were captured using a fluorescence microscope which enabled the dynamic semi-quantitative analysis showed in the plot. At t=39 min, the nanoparticles deposited in the microchannel were collected by an ethanol flush. Those collections were quantified with a fluorescence reader which was the basis of the quantitative analysis presented in the following figures.

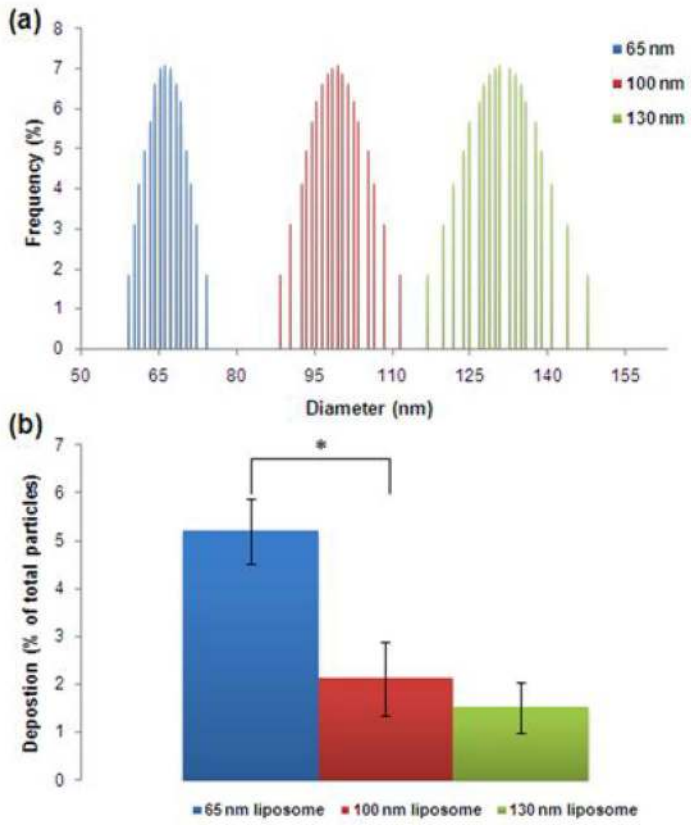

Figure 4. Dependence of the nanoparticle margination on their size

(a) The size distribution of each formulation as measured by dynamic light scattering. **(b)** Comparison of the deposition of 65, 100 and 130 nm in diameter liposomes encapsulating PBS at a flow rate of 50 μL/min (n=3–6; *indicates $p<0.05$; t-test, two-tailed).

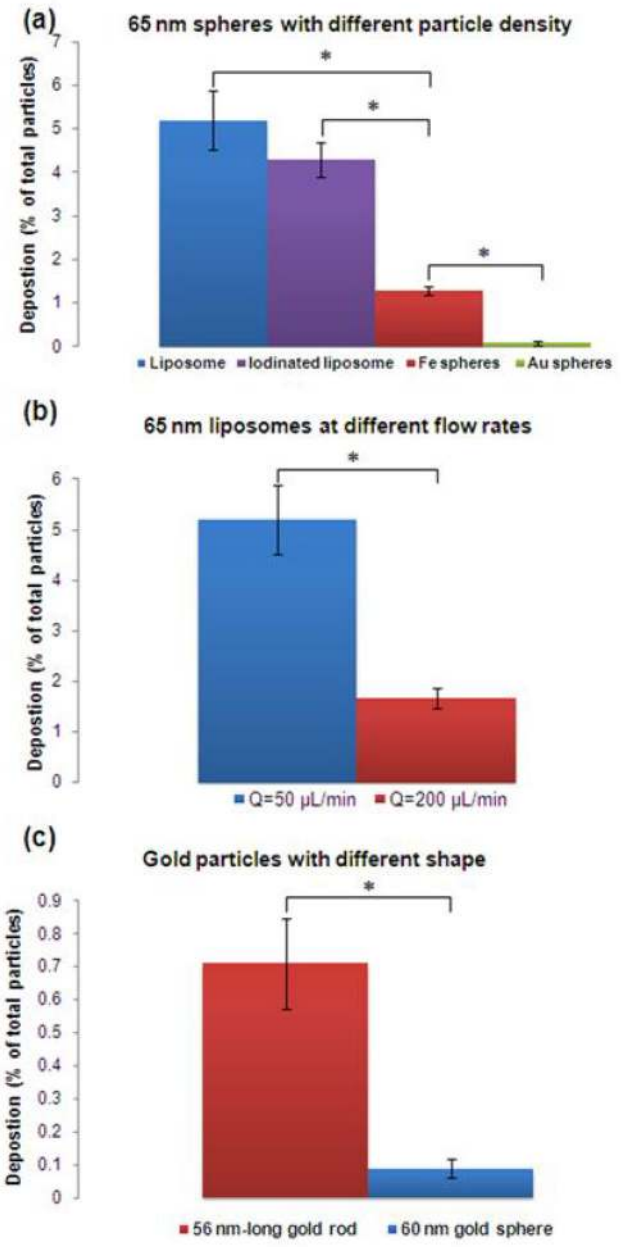

Figure 5. Dependence of the nanoparticle margination on their density and shape

(a) Comparison of the deposition of spheres with a diameter of about 65 nm and different particle density at a flow rate of 50 μL/min. **(b)** Comparison of the deposition of 65 nm liposomes at different flow rates. **(c)** Comparison of the deposition of a 60 nm gold sphere and a 56 nm-long gold rod at a flow rate of 50 μL/min (n=3–6; *indicates $p<0.05$; t-test, two-tailed).

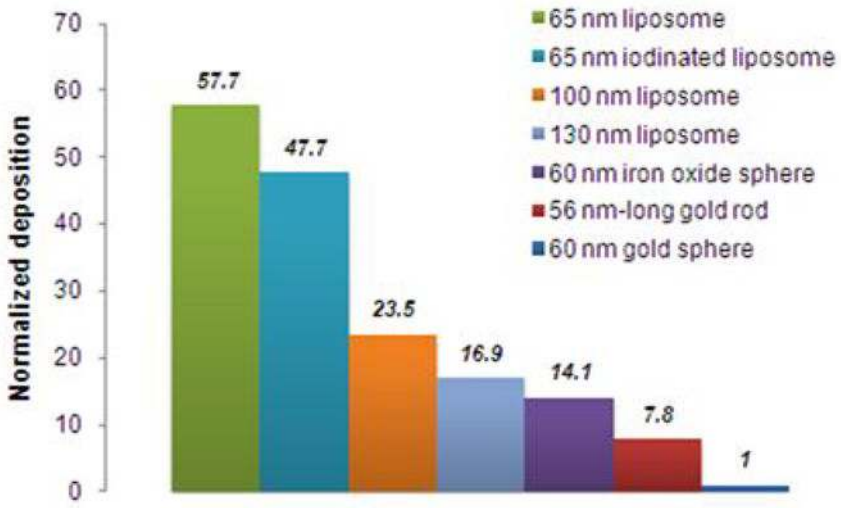

Figure 6.

Overall dependence of the nanoparticle margination on their size, density and shape. The deposition of each nanoparticle was normalized with respect to the particle exhibiting the lowest deposition (i.e. 60 nm gold sphere).

Table 1

Particle characteristics

Formulation	Particle density(g/mL)	Diameter or length(nm)	Aspect ratio(width/length)
130 nm PBS-loaded liposome	1	130	1 (sphere)
100 nm PBS-loaded liposome	1	100	1 (sphere)
65 nm PBS-loaded liposome	1	65	1 (sphere)
65 nm iodine-loaded liposome	2.4	65	1 (sphere)
Iron oxide nanosphere	5.1	60	1 (sphere)
Gold nanosphere	19.3	60	1 (sphere)
Gold nanorod	19.3	56	0.45 (rod)

Table 2

Theoretical estimation of the the diffusion and convection components for each particle

Based on the Stokes-Einstein equation, the diffusion coefficient and the inverse of modified Peclet number was calculated

Formulation	Diffusion coefficient ($\times 10^{-9}$ m^2/s)	$\frac{\text{diffusion}}{\text{momentum}} = \frac{D}{\left(\rho_p/\rho_{water}\right) uL} (\times 10^{-4})$
65 nm PBS-loaded liposome	6.76	5.68
100 nm PBS-loaded liposome	4.39	3.69
130 nm PBS-loaded liposome	3.38	3.52
65 nm iodine-loaded liposome	6.76	2.11
65 nm PBS-loaded liposome *	6.76	1.42
60 nm Fe sphere	7.32	1.20
60 nm Au sphere	7.32	0.31

* The flow rate in this experiment was 4 times faster (200 μL/min) than the rest of the studies (50 μL/min)